of thermally excited carriers), but this is a fundamental limitation for any material without a band gap exceeding k_BT. Nonetheless, such on-off ratios are considered sufficient for logic circuits (*19*), and it is feasible to increase the ratio further by, for example, using p-n junctions, local gates (*3*), or the point contact geometry. However, by analogy to carbon nanotubes (*2*), other, nontransistor applications of this atomically thin material ultimately may prove to be the most exciting.

References and Notes

1. C. D. Dimitrakopoulos, D. J. Mascaro, *IBM J. Res. Dev.* **45**, 11 (2001).
2. R. H. Baughman, A. A. Zakhidov, W. A. de Heer, *Science* **297**, 787 (2002).
3. S. V. Rotkin, K. Hess, *Appl. Phys. Lett.* **84**, 3139 (2004).
4. A. V. Butenko, D. Shvarts, V. Sandomirsky, Y. Schlesinger, *J. Appl. Phys.* **88**, 2634 (2000).
5. M. S. Dresselhaus, G. Dresselhaus, *Adv. Phys.* **51**, 1 (2002).
6. I. L. Spain, in *Chemistry and Physics of Carbon*, P. L. Walker, P. A. Thrower, Eds. (Dekker, New York, 1981), pp. 119–304.
7. O. A. Shenderova, V. V. Zhirnov, D. W. Brenner, *Crit. Rev. Solid State Mater. Sci.* **27**, 227 (2002).
8. A. Krishnan *et al.*, *Nature* **388**, 451 (1997).
9. E. Dujardin, T. Thio, H. Lezec, T. W. Ebbesen, *Appl. Phys. Lett.* **79**, 2474 (2001).
10. H. Shioyama, *J. Mat. Sci. Lett.* **20**, 499 (2001).
11. Other methods of preparing thin graphitic layers exist. The closest analogs of FLG are nanometer-sized patches of graphene on top of pyrolytic graphite (*12*, *13*), carbon films grown on single-crystal metal substrates (*14*), and mesoscopic graphitic disks with thickness down to ~60 graphene layers (*8*, *9*).
12. A. M. Affoune *et al.*, *Chem. Phys. Lett.* **348**, 17 (2001).
13. K. Harigaya, Y. Kobayashi, K. Takai, J. Ravier, T. Enoki, *J. Phys. Cond. Matter* **14**, L605 (2002).
14. T. A. Land, T. Michely, R. J. Behm, J. C. Hemminger, G. Comsa, *Surf. Sci.* **264**, 261 (1992).
15. See supporting data on *Science* Online.
16. J. Kong *et al.*, *Science* **287**, 622 (2000).
17. M. Krüger, I. Widner, T. Nussbaumer, M. Buitelaar, C. Schönenberger, *N. J. Phys.* **5**, 138 (2003).
18. We believe that our thinnest FLG samples (as in Fig. 2A) are in fact zero-gap semiconductors, because small nonzero values of $\delta\varepsilon$ found experimentally can be attributed to inhomogeneous doping, which smears the zero-gap state over a small range of V_g and leads to finite apparent $\delta\varepsilon$.
19. M. R. Stan, P. D. Franzon, S. C. Goldstein, J. C. Lach, M. M. Zeigler, *Proc. IEEE* **91**, 1940 (2003).

20. Supported by the UK Engineering and Physical Sciences Research Council and the Russian Academy of Sciences (S.V.M., S.V.D.). We thank L. Eaves, E. Hill, and O. Shklyarevskii for discussions and interest.

Supporting Online Material

www.sciencemag.org/cgi/content/full/306/5696/666/DC1
Materials and Methods
SOM Text
Figs. S1 to S11
References and Notes

19 July 2004; accepted 15 September 2004

Hydrated Electron Dynamics: From Clusters to Bulk

A. E. Bragg,[1] J. R. R. Verlet,[1] A. Kammrath,[1] O. Cheshnovsky,[2] D. M. Neumark[1,3]*

The electronic relaxation dynamics of size-selected $(H_2O)_n^-/(D_2O)_n^-$ [$25 \leq n \leq 50$] clusters have been studied with time-resolved photoelectron imaging. The excess electron (e_c^-) was excited through the $e_c^-(p) \leftarrow e_c^-(s)$ transition with an ultrafast laser pulse, with subsequent evolution of the excited state monitored with photodetachment and photoelectron imaging. All clusters exhibited p-state population decay with concomitant s-state repopulation (internal conversion) on time scales ranging from 180 to 130 femtoseconds for $(H_2O)_n^-$ and 400 to 225 femtoseconds for $(D_2O)_n^-$; the lifetimes decrease with increasing cluster sizes. Our results support the "nonadiabatic relaxation" mechanism for the bulk hydrated electron (e_{aq}^-), which invokes a 50-femtosecond $e_{aq}^-(p) \rightarrow e_{aq}^-(s^\dagger)$ internal conversion lifetime.

A free electron introduced into a polar solvent, such as water (*1*) or ammonia (*2*), may be trapped by locally oriented solvent molecules. In water, an "equilibrated" hydrated electron [$e_{aq}^-(s)$] can be transiently confined within a roughly spherical cavity defined by six OH bonds oriented toward the negative charge distribution in the so-called Kevan geometry (*3*–*5*). The hydrated electron is an important reagent in condensed-phase chemistry and molecular biology, as it participates in radiation chemistry, electron transfer, and charge-induced reactivity. Thus, research investigating the dynamics of this species, whether in the presence or absence of other reagents, has attracted considerable attention in the theoretical and experimental physical chemistry communities. Here, we present time-resolved results on the electronic relaxation dynamics of anionic clusters of water that lend profound insight to the elucidation of hydrated electron dynamics in the bulk.

The electronic energetics of a hydrated electron are characterized by three types of states (Fig. 1A): a localized $e_{aq}^-(s)$ ground state; three localized, near-degenerate $e_{aq}^-(p)$ excited states; and a delocalized conduction band (CB) characterized by a charge distribution spread across hundreds of molecules in the solvent "network." The visible absorption spectrum of the equilibrium hydrated electron, a broad band peaking at 720 nm (*1*), is well understood as an excitation from the occupied $e_{aq}^-(s)$ state to the vacant $e_{aq}^-(p)$ states (*4*, *5*). The electron-solvent dynamics subsequent to $e_{aq}^-(p) \leftarrow e_{aq}^-(s)$ excitation are more controversial, however, in spite of considerable experimental (*6*–*12*) and theoretical (*13*, *14*) effort devoted to this problem.

Transient absorption measurements made with femtosecond (fs) laser pulses as short as 5 fs (*12*) show a near infrared (NIR) absorption band beyond 900 nm developing on a 40- to 50-fs time scale after $e_{aq}^-(p) \leftarrow e_{aq}^-(s)$ excitation. This broad feature shifts back to shorter wavelengths on a time scale of several hundred fs, with recovery of the original $e_{aq}^-(s)$ absorption spectrum largely complete within ~1 picosecond (ps). Deuteration of the solvent (*8*, *12*) appears only to affect the fastest measured time scale (i.e., the buildup time of the transient NIR absorption), with τ_{D_2O}/τ_{H_2O} = 1.4 to 1.6. As described by Yokoyama *et al.* (*8*), two rather different energy relaxation mechanisms have been proposed to account for these observations. In the "adiabatic solvation" scheme (*13*, *14*), the infrared transient at the earliest times is attributed to absorption of the $e_{aq}^-(p)$ electron, which is solvated on the upper state within 50 fs (process x in Fig. 1A). The excited electron then undergoes internal conversion (IC) to the ground state (y) on a 400-fs time scale, generating ground-state electrons that further relax on the ~1-ps time scale by dissipating energy to the solvent. In contrast, the "nonadiabatic relaxation" mechanism (*7*, *9*, *12*) invokes much more rapid IC, on a 50-fs time scale, and attributes the transient NIR band at early times to absorption of the ground-state electron in a vibrationally excited solvent environment. In this model, subsequent dynamics are assigned to reorganization of the local (~400 fs) and extended (~1 ps) solvent network following the electronic decay.

We present an alternative and complementary approach to assessing the relaxation dynamics of the hydrated electron through time-resolved photoelectron imaging (TRPEI) studies (*15*) of electron dynamics in size-selected water cluster anions, $(H_2O)_n^-$ and $(D_2O)_n^-$, with $25 \leq n \leq 50$. Water cluster anions were first detected mass spectromet-

[1]Department of Chemistry, University of California, Berkeley, CA 94720, USA. [2]School of Chemistry, The Sackler Faculty of Exact Sciences, Tel-Aviv University, 69978 Israel. [3]Chemical Sciences Division, Lawrence Berkeley National Laboratory, Berkeley, CA 94720, USA.

*To whom correspondence should be addressed. E-mail: dan@radon.cchem.berkeley.edu

rically (*16*) and have since been studied with photoelectron (*17–19*), vibrational (*20*), and electronic (*21*) spectroscopies. Cluster studies offer access to structural and dynamic details that are often obscured in the larger, more complex bulk water environment. Because insights gleaned from clusters are meant to extrapolate to the bulk, there is keen interest in determining the size at which "bulk-like" behavior of $(H_2O)_n^-$ clusters becomes apparent (*22*), with the excess electron surrounded by water rather than localized on the cluster surface (*23–25*).

In our TRPEI experiment, described in more detail elsewhere (*26*), water cluster anions are generated in an ion source based on a fast, pulsed molecular beam (*27*) and are mass-selected by time of flight. The mass-selected clusters are investigated with the pump-probe scheme illustrated by the right-most arrows in Fig. 1B. Here, the vertical detachment energy (VDE) is the energy required to remove an electron from an anion while maintaining the anion cluster geometry. We use an ~100-fs laser pulse at 1250 nm (1.0 eV) to excite e_c^-, the excess electron in the cluster anion, from the ground s-state to the excited p-state; this energy lies close to the absorption maximum in the cluster size range investigated here (*21*). After a delay, $\Delta\tau$, during which relaxation may occur, the electron is photodetached by an ultraviolet probe pulse (400 nm or 3.1 eV, ~100 fs) and accelerated by a dc field to an imaging detector composed of a 70-mm-diameter microchannel plate assembly coupled to a phosphor screen.

The state of e_c^- prior to detachment is reflected in its residual velocity afterward, which in turn determines the position the electron strikes on the two-dimensional detector plane. This "velocity map image" (*28*) is then analyzed by two- to three-dimensional inversion, radial integration, and radius-to-energy transformation to yield time-dependent photoelectron kinetic energy (eKE) distributions. Thus, we obtain a time-resolved series of snapshots revealing the dynamics of the nonstationary states created by the pump pulse.

A photoelectron image of $(D_2O)_{25}^-$ acquired within the 1250 nm + 400 nm temporal overlap reveals two features of interest (Fig. 2A). The outermost ring, labeled I, corresponds to the signal with the highest eKE and results from two-color (1250 nm + 400 nm) resonant photodetachment via the $e_c^-(p)$ state (right arrows, Fig. 1B). The next ring, II, is from direct 400-nm detachment of the anion ground state (left arrow, Fig. 1B). Additional features are seen from resonant two-photon and direct one-photon detachment at 1250 nm; however, only features I and II of Fig. 2A show any dependence on pump-probe delay.

The time-resolved photoelectron (TRPE) spectra showing eKE($\Delta\tau$) for features I and II (Fig. 2B) highlight the dynamics that ensue after excitation to the $e_c^-(p)$ cluster state. TRPE spectra of $(D_2O)_{25}^-$ and all other clusters studied here are characterized by depletion and partial recovery in intensity of feature II, with simultaneous growth and decay of feature I. Feature I grows as the pump pulse transfers electronic population to the excited state of the cluster, whereas the depletion of feature II results mainly from this same population transfer. The decay of I and the partial recovery of II are unambiguously assigned to direct electronic relaxation, i.e., internal conversion (IC), from the excited state(s) to the ground state of the cluster. We note that direct one-photon detachment at 1250 nm, the innermost feature in Fig. 2A, is seen for all clusters studied here, which indicates that autodetachment from the pump-excited $e_c^-(p)$ state (requiring no probe pulse) is energetically possible and can, in principle, compete with internal conversion as an excited-state decay pathway. However, this feature shows no time dependence, so excited-state autodetachment appears to be at most a minor relaxation channel.

The integrated intensity of features I and II was plotted versus pump-probe delay and fit to single exponential decay functions convoluted with the instrumental temporal-response (pump-probe temporal cross-correlation, ~150 fs) of the experiment (Fig. 2C). These fits give a $e_c^-(p) \rightarrow e_c^-(s^\dagger)$ relaxation lifetime of 398 ± 50 fs in $(D_2O)_{25}^-$, where $e_c^-(s^\dagger)$ denotes the electron in a vibrationally excited ground state. The shape of feature I remains unchanged even as its intensity evolves, indicating the absence of noticeable hydration dynamics in the $e_c^-(p)$ state before $e_c^-(p) \rightarrow e_c^-(s^\dagger)$ relaxation.

The size and isotope dependence of the electronic decay are evident when the decay traces of excited $(D_2O)_{25}^-$, $(D_2O)_{45}^-$, and $(H_2O)_{45}^-$ are plotted together (Fig. 3). These clusters exhibit excited-state lifetimes of 398 ± 50 fs, 240 ± 25 fs, and 132 ± 10 fs, respectively. For all clusters studied, both sets of isotopomers exhibit shortened excited-state lifetimes with increased cluster size (Fig. 4). Size-dependent isotopomer lifetime ratios, τ_{D_2O}/τ_{H_2O}, for n = 25, 35, and 45 have values of 2.1 ± 0.4, 1.8 ± 0.2, and 1.8 ± 0.2, respectively—similar in magnitude to those

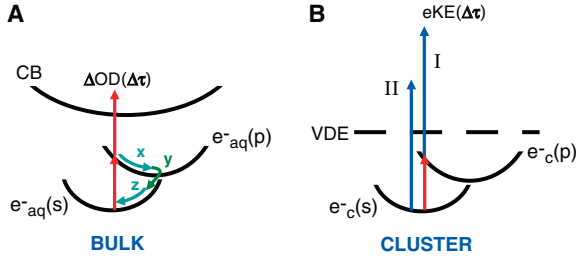

Fig. 1. Energetics of an electron in water. (**A**) The bulk hydrated electron. Red arrows illustrate the transient-absorption schema typically used to study bulk dynamics, in which a time-delayed NIR laser pulse probes the change in optical density [$\Delta OD(\Delta\tau)$] of the sample after an initial infrared excitation. (**B**) Water cluster anions. Levels are similar to those of (A), although the photodetachment continuum replaces the conduction band.

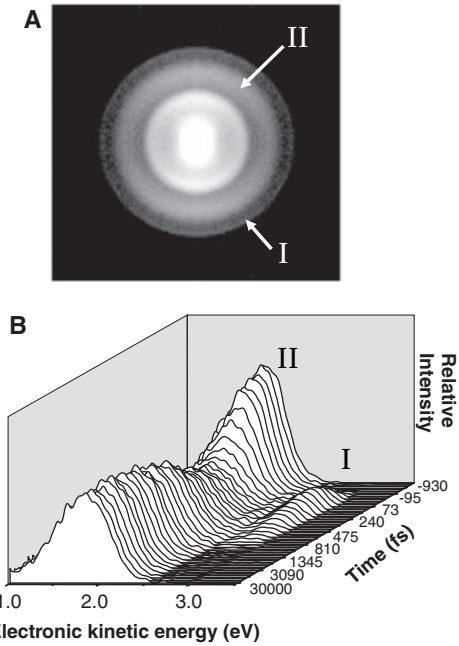

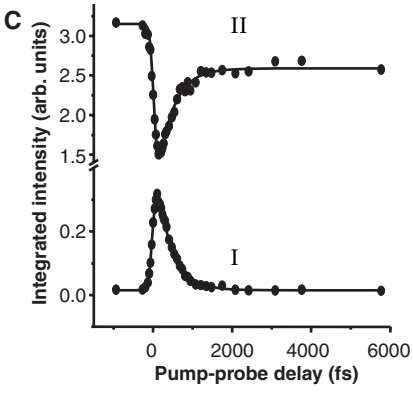

Fig. 2. Time-resolved photoelectron imaging of water cluster anions. (**A**) Photoelectron image of $(D_2O)_{25}^-$ collected at the 1250 nm + 400 nm pump-probe temporal overlap. Features I and II arise from the two-color resonant and direct 400-nm photodetachment processes shown in Fig. 1B. (**B**) Time-resolved photoelectron spectra of $(D_2O)_{25}^-$. Features highlighted in (A) are displayed with pump-probe delays indicated. (**C**) Features I and II. Integrated intensities of features I and II versus pulse delay (experiment, circles; fit, black lines). The fit curves produce a 398 ± 50 fs electronic lifetime for the excited cluster.

observed for the fastest dynamics measured in condensed-phase experiments (*8*, *12*). To test the dependence of the excited-state lifetime on excitation energy, $(H_2O)_{45}^-$ was investigated at a pump energy of 1.57 eV. The lifetime, 117 ± 15 fs, is very close to that found at 1.0 eV and is consistent with the upper bound previously determined by Weber *et al*. (*19*).

These results may be compared and contrasted with the two proposed bulk relaxation mechanisms discussed above. The upper state internal conversion lifetimes decrease markedly with increasing cluster size, approaching 100 fs for the largest $(H_2O)_n^-$ clusters studied here (Fig. 4). This trend suggests even faster IC in bulk water, thereby supporting the nonadiabatic relaxation mechanism in which IC occurs on a 50-fs time scale, rather than the adiabatic solvation model in which a ~400-fs IC has been assigned. Indeed, a plot of IC lifetime versus $1/n$, shown in Fig. 4, is linear and extrapolates to 50 fs in the bulk limit. The significant isotope effect observed for IC in clusters, evident in the $(D_2O)_n^-$ lifetimes plotted in Fig. 4, is likewise consistent with the nonadiabatic mechanism, in which a similar isotope effect is attributed to the IC step (*12*). In contrast, the adiabatic solvation mechanism attributes the isotope effect to faster excited-state hydration in H_2O, whereas the process attributed to IC is insensitive to the identity of the isotopomer (*8*). Finally, the absence of observable upper-state hydration dynamics in our experiment, which would be observed by changes in excited-state spectral features with time, is also in accord with the nonadiabatic mechanism. In this study, all observed dynamical characteristics support the nonadiabatic relaxation model.

A primary motivation for undertaking studies of water cluster anions was to resolve ambiguities regarding the relaxation dynamics of the hydrated electron in solution. We have shown that these ambiguities are directly addressed by investigating the cluster environment, because photoelectron eKE distributions of the excited- and ground-state $(H_2O)_n^-$ are highly distinct (Fig. 2). Thus, internal conversion dynamics from the upper state are cleanly decoupled from solvent relaxation/reorganization processes in the cluster environment, with the rates and nature of relaxation processes free of overlapping spectral signatures that complicate bulk studies. With this in mind, our findings offer important insight into the dynamics of the bulk hydrated electron.

The above interpretation of our results raises the issue of whether it is appropriate to extrapolate bulk hydrated electron dynamics from those of modest-sized water cluster anions. This issue is particularly important in light of debate regarding whether the excess electron is localized at the cluster surface or within a solvent network cavity. Regardless of which structure holds, it certainly appears more reasonable to extrapolate the cluster relaxation rates to the faster of the two assigned IC time scales for the bulk hydrated electron. Nonetheless, extension of our results to the bulk dynamics is more attractive if the clusters studied here have interior excess electrons, because such structures should be more akin to e_{aq}^-. Coe (*22*) has argued that $n^{-1/3}$-dependent plots of $(H_2O)_n^-$ VDEs, obtained from anion photoelectron spectroscopy (n = 11 to 69) (*17*), and absorption maxima, determined from electronic spectroscopy (n = 11 to 50) (*21*), extrapolate sensibly to bulk values and support the notion that clusters in this size range have internal states. This interpretation disagrees with earlier simulations by Barnett *et al*. (*23*) that predict surface states to be more stable up to n = 32, with the transition to interior states occurring by n = 64. However, Bartels (*25*) has pointed out that the model potentials used in these simulations bind the electron too tightly and that improved model potentials for the e^-·H_2O interaction need to be developed to assess the possible role of surface states.

Although our TRPEI measurements do not settle this issue, the IC lifetimes in Fig. 4 vary smoothly with cluster size, casting further doubt on the existence of a structural transition in the n = 25 to 50 range. However, preliminary experiments in our laboratory (*29*) have demonstrated that ion source conditions can be adjusted to generate $(H_2O)_n^-$ ($n \approx 50$) with significantly lower VDEs compared with the clusters discussed here. These newly observed clusters may well represent the long-sought surface states, in which case the cluster dynamics presented in this paper are most likely from structures in which the excess electron has appreciable amplitude within the cluster.

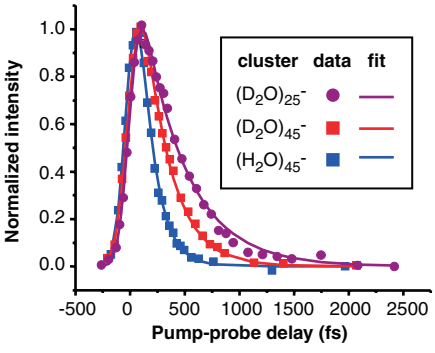

Fig. 3. Size and isotope dependence of excited-state electronic decay traces. Fits (solid lines) to the integrated photoelectron intensities (symbols) versus time yield excited-state lifetimes for $(D_2O)_{25}^-$, $(D_2O)_{45}^-$, and $(H_2O)_{45}^-$ of 398 ± 50 fs, 240 ± 25 fs, and 132 ± 10 fs, respectively.

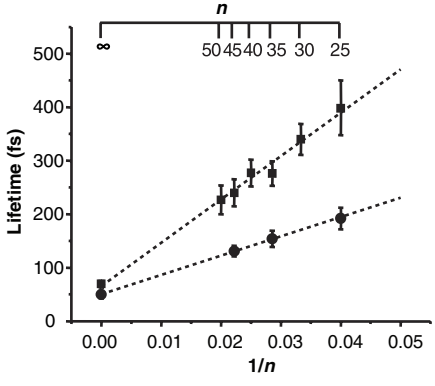

Fig. 4. Size-dependent lifetime trends for $(D_2O)_n^-$ and $(H_2O)_n^-$. Size-dependent decay lifetimes of $(D_2O)_n^-$ (squares) and $(H_2O)_n^-$ (circles) with inverse cluster size ($1/n$). IC lifetimes linearly extrapolate (black dashed lines) to a bulk ($1/n$ = 0) decay time scale of ~50 fs (70 fs) in H_2O (D_2O). Investigated cluster sizes (n) are labeled.

References and Notes

1. E. J. Hart, J. W. Boag, *J. Am. Chem. Soc.* **84**, 4090 (1962).
2. W. Weyl, *Ann. Phys. (Leipzig)* **197**, 601 (1863).
3. L. Kevan, *Acc. Chem. Res.* **14**, 138 (1981).
4. P. J. Rossky, J. Schnitker, *J. Phys. Chem.* **92**, 4277 (1988).
5. M. Boero, M. Parrinello, K. Terakura, T. Ikeshoji, C. C. Liew, *Phys. Rev. Lett.* **90**, 226403 (2003).
6. A. Migus, Y. Gauduel, J. L. Martin, A. Antonetti, *Phys. Rev. Lett.* **58**, 1559 (1987).
7. Y. Kimura, J. C. Alfano, P. K. Walhout, P. F. Barbara, *J. Phys. Chem.* **98**, 3450 (1994).
8. K. Yokoyama, C. Silva, D. H. Son, P. K. Walhout, P. F. Barbara, *J. Phys. Chem. A* **102**, 6957 (1998).
9. A. Hertwig, H. Hippler, A. N. Unterreiner, P. Vohringer, *Ber. Bunsenges. Phys. Chem.* **102**, 805 (1998).
10. M. Assel, R. Laenen, A. Laubereau, *Chem. Phys. Lett.* **317**, 13 (2000).
11. M. J. Tauber, R. A. Mathies, *J. Am. Chem. Soc.* **125**, 1394 (2003).
12. M. S. Pshenichnikov, A. Baltuska, D. A. Wiersma, *Chem. Phys. Lett.* **389**, 171 (2004).
13. B. J. Schwartz, P. J. Rossky, *J. Chem. Phys.* **101**, 6902 (1994).
14. S. Bratos, J. C. Leicknam, D. Borgis, A. Staib, *Phys. Rev. A.* **55**, 7217 (1997).
15. A. Stolow, A. E. Bragg, D. M. Neumark, *Chem. Rev.* **104**, 1719 (2004).
16. M. Armbruster, H. Haberland, H. G. Schindler, *Phys. Rev. Lett.* **47**, 323 (1981).
17. J. V. Coe *et al.*, *J. Chem. Phys.* **92**, 3980 (1990).
18. J. Kim, I. Becker, O. Cheshnovsky, M. A. Johnson, *Chem. Phys. Lett.* **297**, 90 (1998).
19. J. M. Weber *et al.*, *Chem. Phys. Lett.* **339**, 337 (2001).
20. P. Ayotte *et al.*, *J. Chem. Phys.* **110**, 6268 (1999).
21. P. Ayotte, M. A. Johnson, *J. Chem. Phys.* **106**, 811 (1997).
22. J. V. Coe, *Int. Rev. Phys. Chem.* **20**, 33 (2001).
23. R. N. Barnett, U. Landman, C. L. Cleveland, J. Jortner, *J. Chem. Phys.* **88**, 4429 (1988).
24. A. Khan, *J. Chem. Phys.* **118**, 1684 (2003).
25. D. M. Bartels, *J. Chem. Phys.* **115**, 4404 (2001).
26. A. E. Bragg, R. Wester, A. V. Davis, A. Kammrath, D. M. Neumark, *Chem. Phys. Lett.* **376**, 767 (2003).
27. U. Even, J. Jortner, D. Noy, N. Lavie, C. Cossart-Magos, *J. Chem. Phys.* **112**, 8068 (2000).
28. A. T. J. B. Eppink, D. H. Parker, *Rev. Sci. Instrum.* **68**, 3477 (1997).
29. J. R. R. Verlet, A. Kammrath, A. E. Bragg, D. M. Neumark, unpublished data.

30. This research is supported by the National Science Foundation under grant no. CHE-0350585. Additional support from the U.S.-Israel Binational Science Foundation is gratefully acknowledged.

2 August 2004; accepted 27 August 2004
Published online 16 September 2004;
10.1126/science.1103527
Include this information when citing this paper.